

Catalysis Science & Technology

Accepted Manuscript



This is an *Accepted Manuscript*, which has been through the Royal Society of Chemistry peer review process and has been accepted for publication.

Accepted Manuscripts are published online shortly after acceptance, before technical editing, formatting and proof reading. Using this free service, authors can make their results available to the community, in citable form, before we publish the edited article. We will replace this *Accepted Manuscript* with the edited and formatted *Advance Article* as soon as it is available.

You can find more information about *Accepted Manuscripts* in the [Information for Authors](#).

Please note that technical editing may introduce minor changes to the text and/or graphics, which may alter content. The journal's standard [Terms & Conditions](#) and the [Ethical guidelines](#) still apply. In no event shall the Royal Society of Chemistry be held responsible for any errors or omissions in this *Accepted Manuscript* or any consequences arising from the use of any information it contains.

Cite this: DOI: 10.1039/c0xx00000x

www.rsc.org/xxxxxx

ARTICLE TYPE

Activity pattern of metal oxide catalysts in the synthesis of N-phenylpropionamide from propanoic acid and aniline

Francesco Arena^{1,*}, Chiara Deiana², Agata F. Lombardo¹, Pavlo Ivanchenko², Yuriy Sakhno², Giuseppe Trunfio¹, Gianmario Martra^{2,*}

Received (in XXX, XXX) Xth XXXXXXXXX 20XX, Accepted Xth XXXXXXXXX 20XX

DOI: 10.1039/b000000x

The reactivity of various commercial and lab-made oxide samples (e.g., γ -Al₂O₃, CeO₂, ZrO₂, TiO₂) in the heterogeneous catalytic synthesis of N-phenylpropionamide (T, 383K) from aniline and propanoic acid has been investigated. All the studied materials drive the direct synthesis of amide to an extent depending on both chemical and structural properties. A 0th-order kinetic dependence on substrates concentration suggests that the reaction proceeds via a Langmuir-Hinshelwood (L-H) pathway under kinetic control of adsorption-desorption steps (*rate determining step, r.d.s.*). The comparative analysis of activity data on the basis of the relative surface specific kinetic constant discloses a superior surface reactivity of TiO₂, CeO₂, ZrO₂ than γ -Al₂O₃ system, also highlighting marked differences in the catalytic functionality of titania samples. IR spectroscopic studies of carboxylic acids and amine adsorption and interaction patterns show the formation of *bidentate*, *bridging*, and *unidentate* carboxylate intermediates accounting for the different amidation functionality of the studied materials.

1. Introduction

The synthesis of amidic groups is a fundamental class of organic reactions for manufacturing a variety of biological compounds and innovative materials; in particular, beside to widespread uses in the agrochemical industry, ca 65% of drug molecules include, at least, an amide unit,² while amidic groups represent also the backbone of common polymeric materials^{1,2}

Although organic chemistry offers several methods for the lab-scale synthesis of amides, the main industrial manufacture processes still rely on the reaction of amines with pre-activated carboxylic acid precursors, like anhydrides or acid chlorides.^{2,3} In turn, the latter are obtained from thionyl or oxalyl chloride or from carboxylic acid using stoichiometric amounts of coupling reagents (i.e., carbodiimides).² All such methods suffer from severe environmental, safety, and economic drawbacks, included the use of noxious and/or dangerous reagents, and multiple reaction-purification steps resulting in a *poor atom economy*, while large amounts of harmful wastes, requiring special disposal treatments, contribute to high *E-factor*.^{1,2} An alternative method involves the condensation of carboxylic acids with amines at high temperature (>453K), but it is unfeasible for many functionalized substrates.² On this account, the synthesis of amides has been recently indicated as a major Green Chemistry issue²⁻¹⁷

Apart from the recognized effectiveness of microwave irradiation on the condensation of carboxylic acids with amines,^{4,6} and some catalytic redox routes using alternative reagents,^{5,8,9,16} the most attractive option for amides bond formation is the heterogeneous catalytic condensation of amines with carboxylic acids.¹⁰⁻¹⁵ Many solid acids such as boron-organic compounds,⁷ Fe³⁺/K10

montmorillonite,¹⁰ FeCl₃, ZnCl₂, zeolites, and silica-based catalysts,¹¹ sulphated-tungstate,¹² MCM-41,¹³ and Zr-salts,¹⁴ were shown to be active in the synthesis of amides using toluene under “azeotropic distillation” reflux conditions (383K),¹⁻¹⁴ while CeO₂ showed the highest activity among many oxides in various transamidation reactions.¹⁵ In addition, Comerford *et al.* recently reported that silica and SBA materials are highly active in the synthesis of N-(phenyl)-phenylacetamide at 423K in a continuous-flow reactor at short contact time,¹⁷ while mechanistic issues of the condensation of formic and acetic acid with the 1-pentanamine on titania have been recently addressed.¹⁸ In this context, Grosjean *et al.* also emphasized the role of the reaction system showing significant positive effects of heat input on the amidation kinetics because of faster rate of water removal.³

Therefore, this work is aimed at providing a comparative view of the reactivity pattern of various lab-made and commercial oxide catalysts (e.g., γ -Al₂O₃, TiO₂, CeO₂, ZrO₂) in the condensation reaction of aniline with propanoic acid to N-phenylpropionamide using toluene as solvent (T, 383K). The kinetic analysis of activity data reveals that the amidation functionality depends on both chemical and structural properties of the studied materials promoting the formation of different intermediates, probed by IR spectroscopic measurements.

2 Experimental

2.1. Catalysts preparation

Commercial TiO₂ (TiO₂ P25 *Evonik*, ex *Degussa* and TiO₂ *Merck*) and γ -Al₂O₃ (000-1.5E *Akzo Nobel*) powders were used in the “as received” form. The CeO₂ sample was prepared by heating an aqueous solution of the Ce(NH₄)₂(NO₃)₆ precursor

(Sigma-Aldrich, >99%) under continuous stirring and reflux at 373K for 4h. The resulting precipitate was filtered, washed, dried at 373K for two days and finally calcined at 723K for 3h.¹⁹ The ZrO₂ sample was prepared by dissolving the ZrOCl₂·8H₂O precursor (Sigma Aldrich, >99.5%) in distilled water, adding a NaOH solution (0.25 M) at 298K under vigorous stirring. After digestion, the precipitate was filtered, washed until the complete disappearance of chlorides, dried at 373K overnight and further calcined in air at 873K for 3h. The list of the studied samples with the relative codes and specific surface area values is reported in Table 1.

Table 1. List of the studied catalysts

Catalyst Code	Supplier	SSA (m ² /g)
γ-Al ₂ O ₃ (000-1.5E)	Akzo Nobel	261
TiO ₂ _Merck	Merck	10
TiO ₂ _P25	Evonik	55
CeO ₂	Lab-made	90
ZrO ₂	Lab-made	21

2.2. Catalyst characterization

Specific surface area (SSA) values were determined from nitrogen adsorption isotherms (77K) obtained using a ASAP 2010 (Micromeritics Instrument) gas adsorption device. Before measurements the samples were outgassed at 423K until a residual pressure of ca 0.2 mbar. The isotherms were elaborated by the BET method for SSA calculation.

IR spectroscopy measurements were performed using a Bruker Vector 22 spectrometer equipped with a DTGS detector (4 cm⁻¹ resolution); self-supporting pellets (ca 10 mg/cm²) of the catalyst powders were placed into a IR cell with CaF₂ windows and connected to vacuum lines (P<10⁻⁵ mbar) to carry out *in situ* thermal treatments and adsorption-desorption tests.¹⁷ The samples were treated at 723K under dynamic vacuum for 1h, then 6 mbar of O₂ were admitted at the same temperature (1h) for restoring the original oxidation state of the oxides. Subsequently, the samples were cooled down to 473K still under O₂ and, then, to room temperature under vacuum. After collection of the spectra of the treated catalysts in vacuum (*background*), high-purity vapors of propanoic or formic acid and then of 1-pentanamine (Sigma Aldrich) were admitted on the catalysts for IR spectra collection. In the case of the sequential adsorption of propanoic acid and 1-pentanamine a set of measurements was further carried out heating at 383K the pre-saturated samples for 30 minutes. The spectra are reported in Absorbance after subtraction of *background* spectra, while the adsorbed species were analyzed by High Resolution Mass Spectrometry (HR-MS). After spectroscopic measurements the pelletized samples were grounded and suspended in 0.5 mL of Milli-Q water. Subsequently, the suspension was shaken in a Vortex mixer for 15 min and then centrifuged at 10³ rpm for 5 min. The supernatant was then removed and the solid was treated a second time in 0.5 mL of Milli-Q water. Then, the two obtained solutions were mixed and analyzed in a LTQ Orbitrap mass spectrometer (Thermo Scientific) equipped with an atmospheric pressure interface and an electrospray ionization (ESI) source. The source

voltage was set to 4.48 kV. The heated capillary temperature was maintained at 538K. The tuning parameters adopted for the ESI source were: capillary voltage 0.02 V, tube lens 24.77 V; for ions optics: multipole 0 offset, -4.28 V; lens 0 voltage, -4.36 V; multipole 0 offset, -4.28 V; lens 1 voltage, -13.69 V; gate lens voltage, -8.84 V; multipole 1 offset, -18.69 V; front lens voltage, -5.09 V. Mass accuracy of recorded ions (*vs* calculated) was ±1 mmu (without internal calibration). Samples, added of 100 μL of a 0.1M HCOOH aqueous solution, were delivered directly to the mass spectrometer via a Hamilton microliter syringe at constant flow (10 μL/min).

2.3. Catalyst testing

Catalytic tests were carried out in a magnetically stirred three-necks glass flask reactor, operating in batch-mode and equipped with a thermometer, a reflux condenser, and a Dean-Stark device, for continuous water removal by “azeotropic distillation”.³ The reactor was loaded with 10 mL of toluene (solvent), 0.1 mL of n-octane (internal standard), 6 mmol (0.45 g) of propanoic acid and 0.2 g of powdered catalyst (*d_p*<0.1 mm). The suspension was heated at 383K adding slowly, then, a stoichiometric amount of aniline (6 mmol, 0.56 g). Evidences on the absence of internal mass-transfer resistances are given by the *Weisz-Prater* criterion

$$C_{W-P} = \eta \cdot \phi_s^2 = \frac{r_p^2 \cdot (-r)}{D_{An/Tol} \cdot C_{An}} < 3 \cdot 10^{-3} \quad (1)$$

(where *r_p* and (-*r*) are the particle radius (cm) and the rate per unit of volume of catalyst (mol·cm⁻³·h⁻¹), while *D_{An/Tol}* (0.09 cm²·h⁻¹) and *C_{An}* (0.55 mmol·cm⁻³) are the diffusivity and concentration of aniline, respectively), as under the adopted conditions *C_{W-P}* is always orders of magnitude smaller than one.²⁰

Reaction mixture samples were withdrawn from the reactor and analyzed by a GC (7890A-Agilent Technologies) equipped with a capillary column (Restek, Rxi-1ms cross-bond), connected to a FID for determination of propanoic acid and aniline conversion (±3%). Further, after 24h of reaction time the reaction mixture was cooled, filtered by a sintered glass funnel and the catalyst washed with hot ethanol for the complete solubilization of amide, the yield of which was determined by gravimetric analysis after ethanol evaporation.

3 Results and discussion

3.1. Catalytic activity. The results of the catalytic tests in the synthesis of the N-phenylpropanamide at 383K are summarized in Table 2 in terms of aniline and propanoic acid conversion and amide yield values after 24h of reaction time. A preliminary test in absence of catalyst confirms the lack of reactivity of the substrates, while all the oxide catalysts drive the condensation reaction with amide yields comprised between 4 and 47%, in a satisfactory agreement with the conversion degree of both reagents (Table 2). In particular, the lowest and highest yields refer to TiO₂_Merck and TiO₂_P25 samples respectively, while alumina (24%) and ceria (27%) show an intermediate activity, significantly better than ZrO₂ (9%).

These data preliminarily indicate that chemical, structural and textural properties concur to shape the reactivity of the various oxide systems,²¹ although a proper assessment of their amidation functionality deserves the knowledge of kinetic parameters.

Table 2. Conversion data of aniline and propionic acid and *N*-phenylpropionamide yield of the various catalysts at 383K ($C_{PA}=C_{An}$, 0.55 mol/L; C_{cat} , 18 g/L).

Catalyst	Conversion (%) ^a		Amide Yield (%) ^b
	Aniline	P. Acid	
no (blank test)	0	0	0
γ -Al ₂ O ₃ _000-1.5E	22	25	24
TiO ₂ _Merck	5	4	4
TiO ₂ _P25	47	49	47
CeO ₂	28	27	27
ZrO ₂	8	10	9

a) from GC analysis; b) from gravimetric analysis

Then, the kinetic dependence has been properly ascertained by a series of tests conducted at different (stoichiometric) reagents concentration (0.28-1.10 mol/L) and constant TiO₂_P25 catalyst load. The results in Figure 1A show straight-line conversion trends up to an extent of ca. 80%, indicating a very small, if any, kinetic effect of substrates concentration on reaction rate and, thus, a 0th-order kinetic dependence (Fig. 1B). Despite the lack of systematic kinetic data for the other catalysts, this peculiar rate law seems not specific of the TiO₂_P25 system as no changes in reaction rate were also found using doubled concentrations of substrates (1.1 mol/L) and CeO₂ material (36 g/L), while Comerford *et al.* indicate a constant *N*-(phenyl)-phenylacetamide yield (0.34-0.39 g_{cat}⁻¹·h⁻¹) using a K60 silica catalyst in a flow reactor (T, 423K), at various contact time for conversion degrees between 9 and 46%.¹⁷ In particular, this yield values corresponds to a rate of ca. 1.50·10⁻³ mol_{gcat}⁻¹·h⁻¹ that compares to the value of 5.4·10⁻⁴ mol_{gcat}⁻¹·h⁻¹ herein found for TiO₂_P25 at 383K (Fig. 1B).

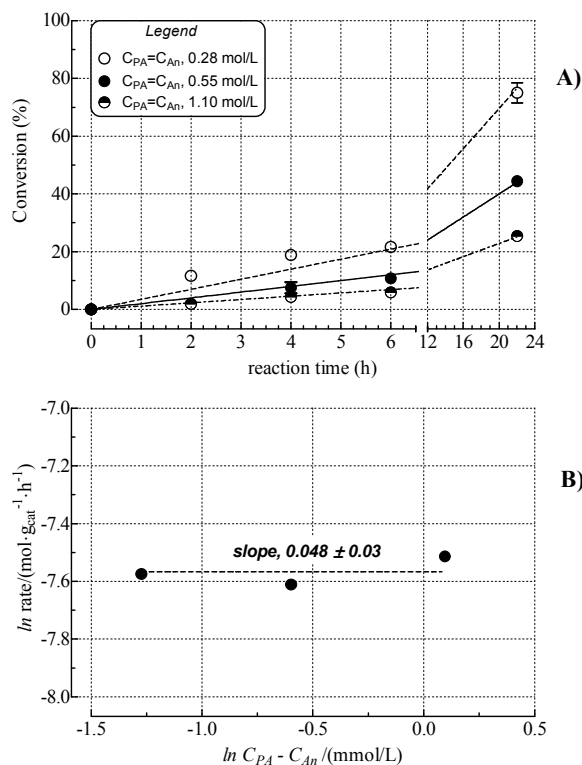


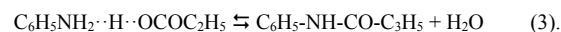
Figure 1. (A) Average conversion of propionic acid and aniline at 383K at different stoichiometric concentrations on TiO₂_P25 catalyst (C_{cat} , 18 g/L); (B) log-plot of rate data vs. reagents concentrations.

These evidences are convincing arguments that the 0th-order kinetic dependence has a general validity irrespective of catalytic materials, likely as a consequence of low operating temperature and characteristics of the “batch” reaction system (i.e., and high reagent-to-catalyst ratio).²²

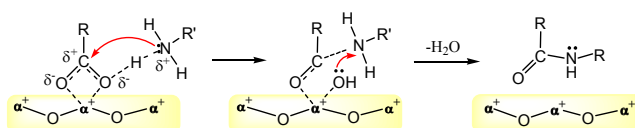
Anyway, in presence of (apolar) toluene as solvent, an acid-base interaction of reacting species drives the primary formation of an adduct,^{3,4}



undergoing a subsequent intramolecular rearrangement leading to formation of the C-N bond and water elimination



The latter requires a proper activation step in order to trigger the nucleophilic attack to the C-atom by the N-atom of the ammine species, this being the *rate determining step* (*r.d.s.*) of the amidation reaction.⁴ In this context, the role of the solid catalyst consists in the adsorption-activation of the adduct on a Lewis acid center (α^+) to restore the nucleophilic character of the nitrogen atom by a weakening of the “N·H” interaction,^{15,18,23} as shown in the below scheme



Scheme 1. Mechanism of the amidation reaction on oxide catalysts.

Having been ascertained an extensive adsorption of carboxylic acids, amines, and amides on surface acidic sites of many oxide materials,^{15,18,23} it can be speculated that the heterogeneous catalytic amidation proceeds *via* a classic Langmuir-Hinshelwood (L-H) reaction pathway,²² although a *dual-site* mechanism, like that of amides transamidation,¹⁵ formaldehyde to methyl formate desmutation,²⁴ and triacylglycerides to fatty methylesters transesterification,²⁵ cannot be ruled out in the light of spectroscopic findings documenting the presence of acid-base pairs on ceria,¹⁵ titania,^{24,26} zirconia and alumina surfaces.²⁴

In turn, the multi-step pathway of the catalytic reaction hinders a straight assessment of the *r.d.s.* because adsorption-desorption processes at the temperature of catalytic tests (383K) can well affect the reaction kinetics.^{15,22,23} Then, at first instance, product desorption is also considered *r.d.s.*



In particular, the above simplified reaction mechanism predicts equilibrium conditions for the adsorption of the adduct on a Lewis acid site (4), while amide formation (5) and desorption (6) steps are considered *r.d.s.* (e.g., $rate=r_5=r_6$) and irreversible due to continuous water evaporation and slow amide desorption,²³ respectively. The active sites balance at steady-state conditions

$$[\alpha^+]_0 = [\alpha^+] + [(RCOO-H_3NR')_{ads}] + [(RCO-NHR')_{ads}] \quad (7)$$

Table 3. 0^{th} -order (k_0) and specific 0^{th} -order constants (k_w , k_{SSA}) of the studied catalysts.

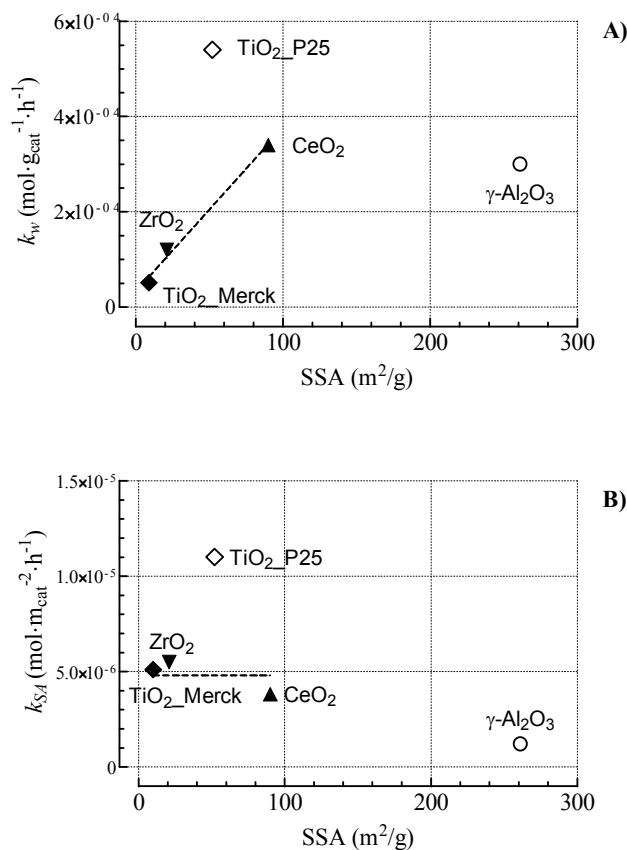
Catalyst	k_0 ($\text{mol}\cdot\text{L}^{-1}\cdot\text{h}^{-1}$)	k_w ($\text{mol}\cdot\text{g}_{\text{cat}}^{-1}\cdot\text{h}^{-1}$)	k_{SSA} ($\text{mol}\cdot\text{m}_{\text{cat}}^{-2}\cdot\text{h}^{-1}$)
TiO ₂ _P25	1.0E-02	5.4E-04	1.0E-05
ZrO ₂	2.1E-03	1.2E-04	5.5E-06
TiO ₂ _Merck	9.2E-04	5.1E-05	5.1E-06
CeO ₂	6.2E-03	3.4E-04	3.9E-06
γ -Al ₂ O ₃	5.5E-03	3.0E-04	1.2E-06

leads to the following kinetic equation

$$\text{rate}(\text{mol}\cdot\text{g}_{\text{cat}}^{-1}\cdot\text{h}^{-1}) = \frac{k_5 \cdot K_4 \cdot [\text{RCOO} - \text{H}_3\text{NR}']}{1 + K_4 \cdot \left(1 + \frac{k_5}{k_6}\right) \cdot [\text{RCOO} - \text{H}_3\text{NR}']} \cdot [\alpha^+]_0 \quad (8),$$

where k_5 (h^{-1}) and k_6 (h^{-1}) are the kinetic constants of the relevant steps, K_4 (L/mol) is the equilibrium constant of adduct adsorption and $[\alpha^+]_0$ (mol/g) the catalyst density of active sites. The eq. 8 proves that the experimental 0^{th} -order kinetic dependence depends on large values of the adsorption constant K_4 that means, in turn, an extensive coverage of active sites by reagents, products, and/or intermediates.

On account of such evidences, the 0^{th} -order constant (k_0 , $\text{mol}\cdot\text{L}^{-1}\cdot\text{h}^{-1}$) has been calculated from conversion data in Table 2, while dividing k_0 by the catalyst concentration (k_w , k_0/C_{cat}) and the latter by surface area values (k_{SSA} , k_w/SSA), the specific constants of the various catalysts per mass and SSA units were obtained, respectively (Table 3).

**Figure 2.** Influence of surface area on: (A) specific 0^{th} -order constant (k_w), and (B) specific surface constant (k_{SSA}) of amide formation (T , 383K) of the various catalysts.

Constant values different by more than one order of magnitude (k_0 , $1.0\cdot 10^{-2}$ - $9.2\cdot 10^{-4}$ $\text{mol}\cdot\text{L}^{-1}\cdot\text{h}^{-1}$) confirm a strong influence of the surface structure on the amidation functionality of the most (TiO₂_P25) and least (TiO₂_Merck) active titania samples.²⁶ However, the influence of surface area on k_w (Fig. 2A) discovers that TiO₂_P25 and γ -Al₂O₃ systems are significantly more and less active than expected from the linear relationship depicted by TiO₂_Merck, ZrO₂ and CeO₂, respectively. Indeed, k_{SSA} values prove that γ -Al₂O₃ ($1.2\cdot 10^{-6}$ $\text{mol}\cdot\text{m}_{\text{cat}}^{-2}\cdot\text{h}^{-1}$) and TiO₂_P25 ($1.0\cdot 10^{-5}$ $\text{mol}\cdot\text{m}_{\text{cat}}^{-2}\cdot\text{h}^{-1}$) have the worst and best functionality respectively, while TiO₂_Merck, ZrO₂ and CeO₂ are characterized by an intermediate reactivity, probed by similar k_{SSA} values, *ca.* five times larger than γ -Al₂O₃ (Fig. 2B).

The origin of the different reactivity of the studied oxides is addressed by IR measurements.

3.2. IR spectroscopy and mechanistic evidences. The amidation functionality of the various catalysts has been probed by a systematic IR study of propanoic acid adsorption and its reaction pattern toward 1-pentanamine (*taken as model amine for the sake of safety*). The spectral data of the various oxides are shown in Figure 3, while a summary of the various signals is reported in Table S1 of SI. In all the cases the adsorption of propanoic acid (*blue lines*) yields the formation of carboxylate species, according to the $\nu_{\text{asym}}\text{COO}^-$ and $\nu_{\text{sym}}\text{COO}^-$ modes in the 1650-1550 and 1450-1400 cm^{-1} ranges, respectively.²⁷

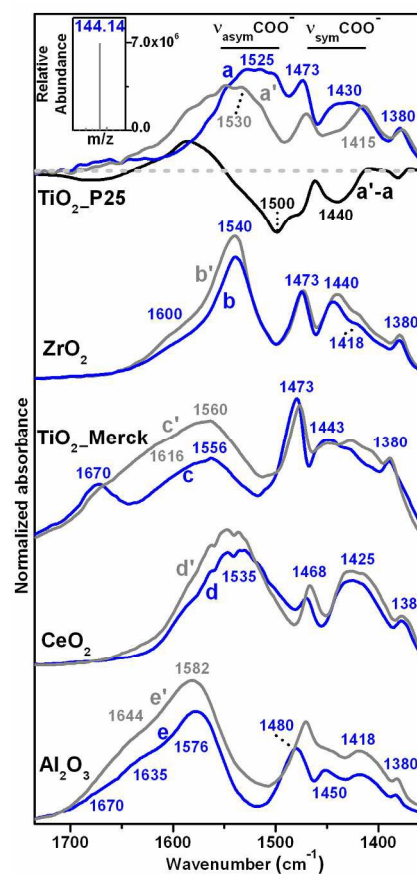
**Figure 3.** IR spectra of TiO₂_P25, ZrO₂, TiO₂_Merck, CeO₂, and γ -Al₂O₃ contacted with propanoic acid and outgassed at r.t. (blue lines: a, b, c, d, e); and after admission of 1-pentanamine (grey lines: a', b', c', d', e'). Black curve of TiO₂_P25 results from a'-a curves subtraction.

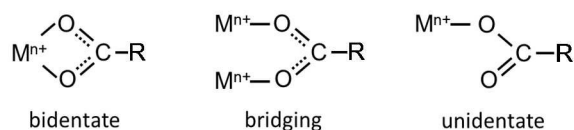
Table 4. Splitting between $\nu_{\text{asym}}\text{COO}^-$ and $\nu_{\text{sym}}\text{COO}^-$ modes of propanoate species on the various catalysts and in the sodium salt for comparison.

Catalyst	$\nu_{\text{asym}}\text{COO}^-$	$\nu_{\text{sym}}\text{COO}^-$	$\Delta\nu$
TiO ₂ _P25	1500	1440	63
ZrO ₂	1540	1440	100
TiO ₂ _Merck	1556	1443	113
CeO ₂	1535	1425	110
γ -Al ₂ O ₃	1576	1450	126
C ₂ H ₅ COONa	1560	1430	130

In the case of TiO₂_Merck and γ -Al₂O₃ also the $\nu\text{C}=\text{O}$ component of the carboxylic group of C₂H₅COOH molecules in the non-dissociated form is present (ca 1670 cm⁻¹). Moreover, the pattern in the case of CeO₂ is visibly shifted to lower frequency, probably reflecting the peculiar electronic properties of lanthanides.²⁸

The subsequent admission of 1-pentanamine on TiO₂_P25 (Fig. 3a') causes a decrease of components due to propanoate species and the appearance of a tail in the 1650-1560 cm⁻¹ range due to the $\nu\text{C}=\text{O}$ mode of amide species.^{29,30} The formation of amide was confirmed by HR-MS of the washing solution of the TiO₂_P25 sample, showing a signal at $m/z=144.14$ due to the protonated N-pentylpropanamide (Fig. 3, top-left inset). For all the other systems the adsorption of amine results in the superimposition of its IR pattern and no N-pentylpropanamide was detected in the washing solutions by HR-MS.

Further, the IR signals of adsorbed propanoic acid due to the carboxylate moieties appear to be composed of sub-bands, position and relative intensity of which are characteristic for each oxide. Although the broadness of the overall $\nu_{\text{asym}}\text{COO}^-$ pattern of TiO₂_P25, TiO₂_Merck and CeO₂ hinders any reliable deconvolution of the various components, the difference between the spectra of TiO₂_P25, after and before the amidation, indicates that the $\nu_{\text{asym}}\text{COO}^-$ and $\nu_{\text{sym}}\text{COO}^-$ components vanishing during the reaction are centered at 1500 and 1440 cm⁻¹, respectively (Fig. 3, curve a'-a). These data provide a splitting value of only 60 cm⁻¹, markedly lower than that of a ionic carboxylate like C₂H₅COONa (Table 4), suggesting, thus, the prevalent formation on this system of a *bidentate* carboxylate structure (Scheme 2).²⁷



Scheme 2. Carboxylate structures stabilized on oxide surface with M^{n+} being the metal (e.g., Ti^{4+} , Zr^{4+} , Ce^{4+} , Al^{3+}) cation (ref. 27).

The lack of straight correlations in the evolution of sub-bands at high and low frequencies hinders the recognition of $\nu_{\text{asym}}\text{COO}^-$ and $\nu_{\text{sym}}\text{COO}^-$ pairs in the other cases. Anyway, it can be considered that i) the angle between the two branches of $-\text{COO}^-$ oscillators is expected to be larger than 90°, and ii) in both *bridging* and *bidentate* structures such oscillators can be reasonably assumed sufficiently equivalent in order to apply the well-known relationship

$$(I_{\text{sym}}/I_{\text{asym}}) = \text{ctg}^2(\theta/2) \quad (9)$$

where θ is the angle between the two branches.³¹ As a consequence, in each pair of signals the one due to the $\nu_{\text{asym}}\text{COO}^-$ mode should exhibit a higher intensity with respect to the $\nu_{\text{sym}}\text{COO}^-$ partner. On such a basis, the most intense components of the $\nu_{\text{sym}}\text{COO}^-$ patterns observed for the adsorption of propanoic acid on catalysts other than TiO₂_P25 should be paired to the most intense $\nu_{\text{asym}}\text{COO}^-$ ones. calculated $\Delta\nu$ splitting values (Table 4) indicate that the prevailing fraction of carboxylate groups should be of *bridging* type (Scheme 2) on ZrO₂, TiO₂_Merck, CeO₂ and γ -Al₂O₃. The formation of different amounts of carboxylate species on titania samples is still to be related to the surface features of TiO₂_P25 and TiO₂_Merck materials.²⁶

Although different intermediates and activity evidences confirm the superior amidation functionality of the TiO₂_P25 sample, these data do not provide information on differences among the other catalysts, as they are all inactive toward amidation under the “model” *in situ* conditions and at room temperature.

On this account, the catalysts subjected to the adsorption of propanoic acid and 1-pentanamine were heated at 383K and further cooled down to r.t. for IR measurements (Fig. S1 of SI). TiO₂_P25 shows a further consumption of the components of carboxylate moieties, while the weak band at 1630 cm⁻¹ rises in intensity, being due to the $\nu\text{C}=\text{O}$ mode of the amide group.^{29,30} Negligible changes in the spectral pattern of γ -Al₂O₃ still match its poor catalytic functionality, while a strong decrease of all the signals hinders any reliable assessment of the various species on ZrO₂, TiO₂_Merck and CeO₂ samples, being likely the consequence of significant desorption (*and condensation on colder points of the IR cell*) phenomena.

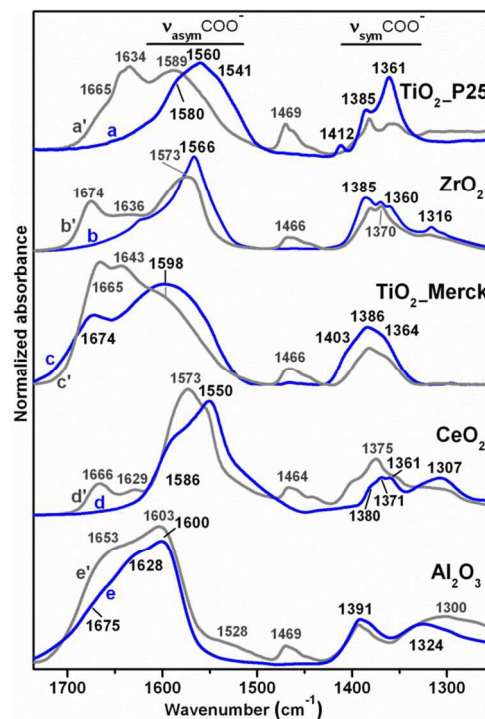


Figure 4. IR spectra of TiO₂_P25, ZrO₂, TiO₂_Merck, CeO₂, and γ -Al₂O₃ contacted with formic acid and outgassed at r.t. (blue lines: a, b, c, d, e); and after admission of 1-pentanamine (grey lines: a', b', c', d', e').

Then, a series of measurements was carried out using formic acid, since it is expected to be more reactive because of the lack of inductive effects of the alkyl substituent.¹⁸ The spectral features of formic acid adsorption (Fig. 4, blue lines) account for the formation of the carboxylate species on TiO₂_P25, ZrO₂ and CeO₂ (typical $\nu_{\text{asym}}\text{COO}^-$ and $\nu_{\text{sym}}\text{COO}^-$ pattern in the 1600-1500 and 1400-1300 cm⁻¹ ranges, respectively), shifted to lower frequency for CeO₂ (*vide supra*). The components of HCOOH molecules in non-dissociated form in the spectra of TiO₂_Merck and γ -Al₂O₃ are also evident. A summary of the assignment of the signals on the various catalysts is reported in Table S2 of SI. The admission of 1-pentanamine causes a decrease of the components due to formates and the appearance of signals in the range of 1700-1600 cm⁻¹, due to the $\nu\text{C}=\text{O}$ mode of amide species,^{29,30} except for the γ -Al₂O₃, where the admission of the amine basically gives rise only to the appearance of the spectral pattern of newly adsorbed molecules. At the opposite, TiO₂_P25 shows the strongest decrease of the $\nu_{\text{asym}}\text{COO}^-$ and $\nu_{\text{sym}}\text{COO}^-$ signals. Notably, on the whole these data are in a fairly good agreement with the activity scale (TiO₂_P25 > ZrO₂ \approx TiO₂_Merck \approx CeO₂ > γ -Al₂O₃) of amidation tests (Fig. 2).

As already observed in the case of propanoic acid, also the spectral features of formate species result from the overlapping of sub-bands, despite in several cases they are better resolved. In addition, the absence of the signal due to the deformation modes of -CH₂ and -CH₃ groups allows for a more clear recognition of the $\nu_{\text{asym}}\text{COO}^-$ and $\nu_{\text{sym}}\text{COO}^-$ patterns. Thus, a deconvolution analysis of the formate patterns has been performed, setting the position of the various components by the 2nd-derivative method (Fig. 5).³² For the broad and featureless $\nu_{\text{asym}}\text{COO}^-$ band observed on TiO₂_Merck no significant information was provided by such method; in such a case the overall contribution of the formate species with respect to HCOOH ones, responsible of the component at 1674 cm⁻¹, was evaluated, gathering all possible $\nu_{\text{asym}}\text{COO}^-$ signals in one component (centered at 1598 cm⁻¹). As a consequence, the possibility to establish correlations between specific $\nu_{\text{asym}}\text{COO}^-$ and $\nu_{\text{sym}}\text{COO}^-$ components was prevented; yet, two limit pairing possibilities of the $\nu_{\text{asym}}\text{COO}^-$ components at lower frequency can be considered, always taking into account the criterion based on the relative intensity of $\nu_{\text{asym}}\text{COO}^-$ and $\nu_{\text{sym}}\text{COO}^-$ signals reported above:

- the pairing with $\nu_{\text{sym}}\text{COO}^-$ component at lowest frequency, resulting in the maximum $\Delta\nu$ with respect the $\nu_{\text{asym}}\text{COO}^-$;
- the pairing with $\nu_{\text{sym}}\text{COO}^-$ component at highest frequency, resulting in the minimum $\Delta\nu$ with respect the $\nu_{\text{asym}}\text{COO}^-$. On this account, the type i) pairing of $\nu_{\text{asym}}\text{COO}^-$ components at 1541 and 1519 cm⁻¹ obtained for TiO₂_P25 with the $\nu_{\text{sym}}\text{COO}^-$ component at 1361 cm⁻¹ provide a $\Delta\nu$ splitting of 180 and 158 cm⁻¹; they can be related to *bridging/bidentate* and *bidentate* formate species respectively, as HCOONa exhibits a $\Delta\nu$ splitting of 201 cm⁻¹.²⁷

In the case of ZrO₂, the recognition of components due to *bridging/bidentate* formates might result only from pairing of type ii) between the $\nu_{\text{asym}}\text{COO}^-$ component at 1550 cm⁻¹ and the highest frequency $\nu_{\text{sym}}\text{COO}^-$ component at 1370 cm⁻¹ ($\Delta\nu$, 180 cm⁻¹).

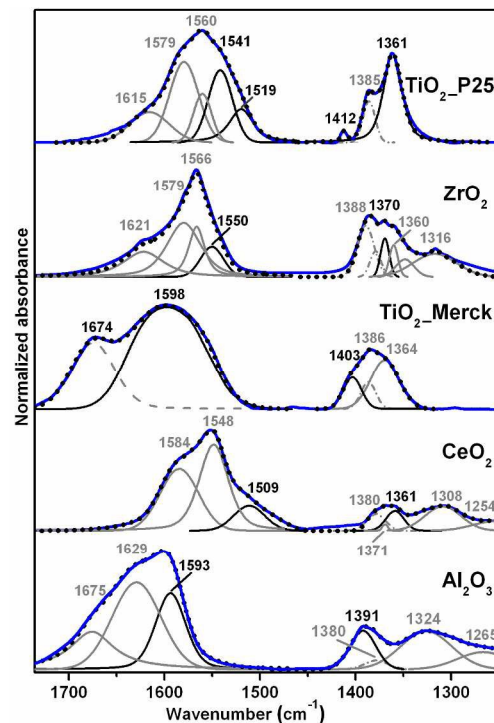


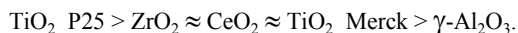
Figure 5. IR spectra (Fig. 4; blue lines) and deconvolution analysis by the components relative to bridging, bidentate and unidentate formate species (a, b, c - grey lines) with the relative predicted spectrum (dotted black line).

The same occurs by considering components at 1548 and 1371-1361 cm⁻¹ for CeO₂ ($\Delta\nu$, 177-187 cm⁻¹, *bridging/bidentate*); the presence of *bidentate* formate might be indicated by the pairing between $\nu_{\text{asym}}\text{COO}^-$ components at 1509 cm⁻¹ with the $\nu_{\text{sym}}\text{COO}^-$ components at 1371-1361 cm⁻¹ ($\Delta\nu$, 138-148 cm⁻¹). In any case, the $\nu_{\text{asym}}\text{COO}^-$ components of *bridging/bidentate* and *bidentate* formates on both ZrO₂ and CeO₂ constitute a small fraction of the overall $\nu_{\text{asym}}\text{COO}^-$ pattern in comparison to TiO₂_P25. Finally, the narrowest $\Delta\nu$ splitting of 202 cm⁻¹ (1593-1391 cm⁻¹) calculated for γ -Al₂O₃ indicates the presence of *bridging* formates whilst *bidentate* species can be excluded.²⁷ Also the main $\nu_{\text{asym}}\text{COO}^-$ component at 1629 cm⁻¹ can be attributed to *bridging* species if paired with the $\nu_{\text{sym}}\text{COO}^-$ component at 1391 cm⁻¹ ($\Delta\nu=238$ cm⁻¹), or even to *unidentate* species (Scheme 2) if $\nu_{\text{sym}}\text{COO}^-$ at lower frequency are considered. For TiO₂_Merck the $\nu_{\text{sym}}\text{COO}^-$ at higher frequency is centered at 1403 cm⁻¹, while the broad $\nu_{\text{asym}}\text{COO}^-$ pattern extends down to 1515 cm⁻¹, indicating that *bidentate* formates might be present. However, considering the maximum at 1598 cm⁻¹, a $\Delta\nu$ of 195 cm⁻¹ suggests a prevalent presence of *bridging* formates. As for propanoic acid, the different amount of the various types of formates on TiO₂_P25 and TiO₂_Merck are still related to their significantly different surface structure.²⁶ Additional evidences on the different structure of formates on the two titania catalysts are obtained from the ratio between the sum of the integrated intensities of all the $\nu_{\text{sym}}\text{COO}^-$ components (I_{sym}) and the analogous for $\nu_{\text{asym}}\text{COO}^-$ (I_{asym}). The values obtained were 0.3 and ca 0.2 for TiO₂_P25 and TiO₂_Merck respectively, representing the *average* $I_{\text{sym}}/I_{\text{asym}}$

value for the various types of formates present in the two cases. It is worthwhile to notice that the data base for such calculation (Table S3 in SI) was obtained by minimizing the contribution of the $\delta_{\text{O-C-H}}$ mode in the deconvolution of the 1450-1300 cm^{-1} pattern in the case of TiO_2 _Merck and, viceversa, maximizing it in the case of TiO_2 _P25. The above values of the $I_{\text{sym}}/I_{\text{asym}}$ ratio can be then considered as the closest ones within the variability of the fitting procedure. The average angle between the C-O moieties of formates on TiO_2 _P25 and TiO_2 _Merck results to be ca 120° and 130° , respectively.³¹ These values are consistent with those reported by Deacon and Phillips for a series of acetate complexes (Fig. S2 in SI).²⁸ In fact, only *bridging* species feature angles larger than 123° ; then, also considering the differences between acetates and formates, it can be argued that *bridging* species might be prevalent on TiO_2 _Merck. Angle values in the range of 118 - 123° appeared common to *bridging* and *bidentate* acetates, while the latter selectively exhibit angles between 118 and 109° ; thus, an *average* value of 120° for formates on TiO_2 _P25 well accounts for a mixture of formate structures containing significant amounts of *bidentate* formates.

4 Conclusions

- The reactivity of various catalytic oxide materials (T, 383K) in the direct synthesis of N-phenylpropionamide from propanoic acid and aniline has been assessed.
- Chemical and surface properties determine the amidation functionality of the studied systems:



- A 0^{th} -order kinetic dependence is related to a Langmuir-Hinshelwood reaction path under kinetic control of product-desorption step.
- The reactivity of the studied oxides matches their ability in stabilizing *bidentate* carboxylate intermediates.
- Bidentate* carboxylates are much more reactive towards the nucleophilic attack of amines than both *bridging* and *unidentate* species.

Acknowledgements

The University of Torino and the Compagnia di San Paolo are acknowledged for funding (Project No. ORTO11RRT5). Dr. Marco Pazzi is gratefully acknowledged for HR-MS analysis.

Notes and references

^a Dipartimento di Ingegneria Elettronica, Chimica e Ingegneria Industriale, Università degli Studi di Messina, Viale F. Stagno D'Alcontres 31, 98166 Messina, Italy. Fax: +39 090 391518; Tel: +39 090 393134; E-mail: Francesco.Arena@unime.it

^b Department of Chemistry and Centre for "Nanostructured Interfaces and Surfaces-NIS", University of Torino, via P. Giuria 7, 10125 Torino, Ital; E-mail: Gianmario.Martra@unito.it

† Electronic Supplementary Information (ESI) available: [details of any supplementary information available should be included here]. See DOI: 10.1039/b000000x/

‡ Footnotes should appear here. These might include comments relevant to but not central to the matter under discussion, limited experimental and spectral data, and crystallographic data.

- K. Ishihara, *Tetrahedron*, 2009, **65**, 1085.
- V.R. Pattabiraman, J.W. Bode, *Nature*, 2011, **480**, 471.
- C. Grosjean, J. Parker, C. Thirsk, A.R. Wright, *Organic Process Research & Development*, 2012, **16**, 781.
- L. Perreux, A. Loupy, F. Volatron, *Tetrahedron*, 2002, **58**, 2155.
- Khalafi-Nezhad, A. Parhami, M.N. Soltani Rad, and A. Zarea *Tetrahedron Letters*, 2005, **46**, 6879.
- E. Gelens, L. Smets, L.A.J. Sliedregt, B.J. van Steen, C.G. Kruse, R. Leurs, R.V.A. Orru, *Tetrahedron Letters*, 2005, **46**, 3751.
- K. Arnold, A.S. Batsanov, B. Davies, A. Whiting, *Green Chemistry*, 2008, **10**, 124.
- Kumar, H.K. Akula, M.K. Lakshman, *European Journal of Organic Chemistry*, 2010, 2709.
- B. Gnanaprakasam, D. Milstein, *Journal of the American Chemical Society*, 2011, **133**, 1682.
- K.V.N.S. Srinivas, B. Das, *Journal of Organic Chemistry*, 2003, **68**, 1165.
- J.W. Comerford, J.H. Clark, D.J. Macquarrie, S.W. Breeden *Chemical Communications*, 2009, 2562.
- P.S. Chaudhari, S.D. Salim, R.V. Sawant, K.G. Akamanchi, *Green Chemistry*, 2010, **12**, 1707.
- K. Komura, Y. Nakano, M. Koketsu, *Green Chemistry*, 2011, **13**, 828.
- C.L. Allen, A.R. Chhatwal, J.M.J. Williams, *Chemical Communications*, 2012, **48**, 666.
- M. Tamura, T. Tonomura, K. Shimizu, A. Satsuma, *Green Chemistry*, 2012, **14**, 717.
- J. Soulè, H. Miyamura, S. Kobayashi, *Journal of the American Chemical Society*, 2011, **133**, 18550.
- J.W. Comerford, T.J. Farmer, D.J. Macquarrie, S.W. Breeden, J.H. Clark, ARKIVOC-2012 (vii) 282-293.
- C. Deiana, Y. Sakhno, M. Fabbiani, M. Pazzi, M. Vincenti, G. Martra *ChemCatChem*, 2013, **5**, 2832.
- H. Zou, Y.S. Lin, N. Rane, T. He, *Industrial Engineering Chemistry Research*, 2004, **43**, 3019.
- H.S. Fogler, *Elements of Chemical Reaction Engineering* (4th Ed.), 2006 Pearson Education, Inc., p. 839.
- G. Busca, *Physical Chemistry Chemical Physics*, 1999, **1**, 723.
- Chorkendorff, J.W. Niemantsverdriet, *Concepts of Modern Catalysis and Kinetics*, WILEY-VCH GmbH & Co. KGaA, Weinheim, 2005.
- L.-F. Liao, C.-F. Lien, D.-L. Shieh, F.-C. Chen, J.-L. Lin, *Physical Chemistry Chemical Physics*, 2002, **4**, 4584.
- A. Parmaliana, F. Frusteri, F. Arena, A. Mezzapica, V. Sokolovskii, *Catalysis Today*, 1998, **46**, 117.
- C. Cannilla, G. Bonura, F. Arena, E. Rombi, F. Frusteri, *Catalysis Today*, 2012, **195**, 32.
- G. Martra, *Applied Catalysis A*, 2000, **200**, 275.
- K. Nakamoto, *Infrared and Raman Spectra of Inorganic and Coordination Compounds*, Wiley, New York, 1986, 4th ed., p. 232–233.
- G.B. Deacon, R.J. Phillips, *Coordination Chemistry Reviews*, 1980, **33**, 227.
- N. B. Colthup, L. H. Daly, S. E. Wiberley, *Introduction to Infrared and Raman Spectroscopy*, 2nd ed., Academic Press, New York, 1975, p. 321 and 225.
- X.G. Chen, R. Schweitzerstenner, S.A. Asher, N.G. Mirkin, S. Krimm, *Journal of Physical Chemistry*, 1995, **99**, 3074.

-
31. . P.S. Braterman, *Metal Carbonyl Spectra*, Academic Press, London, 1975, p. 64.
 32. J.M. Chalmers, P.R. Griffiths, Eds., *Handbook of Vibrational Spectroscopy*, Wiley, 2001, vol. 3, p. 64.